

# Estimation and Spatio-temporal Patterns of Carbon Emissions from Grassland Fires in Inner Mongolia, China

YU Shan<sup>1,2</sup>, JIANG Li<sup>2</sup>, DU Wala<sup>3</sup>, ZHAO Jianjun<sup>1,4</sup>, ZHANG Hongyan<sup>1,4</sup>, ZHANG Qiaofeng<sup>2</sup>, LIU Huijuan<sup>3</sup>

(1. *Key Laboratory of Geographical Processes and Ecological Security in Changbai Mountains, Ministry of Education, School of Geographical Sciences, Northeast Normal University, Changchun 130024, China*; 2. *School of Geographical Sciences, Inner Mongolia Normal University, Hohhot 010022, China*; 3. *Grassland Research Institute, Chinese Academy of Agricultural Sciences, Hohhot 010010, China*; 4. *Urban Remote Sensing Application Innovation Center, School of Geographical Sciences, Northeast Normal University, Changchun 130024, China*)

**Abstract:** Grassland fires results in carbon emissions, which directly affects the carbon cycle of ecosystems and the carbon balance. The grassland area of Inner Mongolia accounts for 22% of the total grassland area in China, and many fires occur in the area every year. However, there are few models for estimation of carbon emissions from grassland fires. Accurate estimation of direct carbon emissions from grassland fires is critical to quantifying the contribution of grassland fires to the regional balance of atmospheric carbon. In this study, the regression equations for aboveground biomass (AGB) of grassland in growing season and MODIS NDVI (Normalized Difference Vegetation Index) were established through field experiments, then AGB during Nov.–Apr. were retrieved based on that in Oct. and decline rate, finally surface fuel load was obtained for whole year. Based on controlled combustion experiments of different grassland types in Inner Mongolia, the carbon emission rate of grassland fires for each grassland type were determined, then carbon emission was estimated using proposed method and carbon emission rate. Results revealed that annual average surface fuel load of grasslands in Inner Mongolia during 2000–2016 was approximately  $1.1978 \times 10^{12}$  kg. The total area of grassland which was burned in the Inner Mongolia region over the 17-year period was 5298.75 km<sup>2</sup>, with the annual average area of 311.69 km<sup>2</sup>. The spatial distribution of grassland surface fuel loads is characterized by decreasing from northeast to southwest in Inner Mongolia. The total carbon emissions from grassland fires amounted to  $2.24 \times 10^7$  kg with an annual average of  $1.32 \times 10^6$  for the study area. The areas with most carbon emissions were mainly concentrated in Old Barag Banner and New Barag Right Banner and on the right side of the Oroqin Autonomous Banner. The spatial characteristics of carbon emission depend on the location of grassland fire, mainly in the northeast of Inner Mongolia include Hulunbuir City, Hinggan League, Xilin Gol League and Ulanqab City. The area and spatial location of grassland fires can directly affect the total amount and spatial distribution of carbon emissions. This study provides a reference for estimating carbon emissions from steppe fires. The model and framework for estimation of carbon emissions from grassland fires established can provide a reference value for estimation of carbon emissions from grassland fires in other regions.

**Keywords:** grassland fires; surface fuel load; area burned; estimation of carbon emissions; Inner Mongolia, China

**Citation:** YU Shan, JIANG Li, DU Wala, ZHAO Jianjun, ZHANG Hongyan, ZHANG Qiaofeng, LIU Huijuan, 2020. Estimation and Spatio-temporal Patterns of Carbon Emissions from Grassland Fires in Inner Mongolia, China. *Chinese Geographical Science*, 30(4): 572–587. <https://doi.org/10.1007/s11769-020-1134-z>

Received date: 2019-12-16; accepted date: 2020-04-07

Foundation item: Under the auspices of National Natural Science Foundation of China (No. 41761101, 41771450, 41871330), National Natural Science Foundation of Inner Mongolia (No. 2017MS0409), Fundamental Research Funds for the Central Universities (No. 2412019BJ001)

Corresponding author: ZHANG Hongyan. E-mail: zhy@nenu.edu.cn

© Science Press, Northeast Institute of Geography and Agroecology, CAS and Springer-Verlag GmbH Germany, part of Springer Nature 2020

## 1 Introduction

In recent years, the rapid increase in the concentrations of carbonaceous greenhouse gases (carbon dioxide (CO<sub>2</sub>) and methane (CH<sub>4</sub>)) has become a primary factor contributing to global warming. These two gases account for over 70% of the total greenhouse gas effect (Rodhe, 1990; Flannigan and Wagner, 1991). A multi-fold increase in the concentrations of these two gases may result in global climate change, more frequent occurrences of grassland fires, and an increase in fire intensity, areas destroyed and carbon emissions, which will have a profound impact on the Earth's ecosystems and human environments. Currently, direct carbon emissions from grassland fires worldwide amount to approximately  $2.0 \times 10^{12}$  kg/yr (Van der Werf et al., 2010). As the greenhouse effect has become better understood, CO<sub>2</sub> emissions from grassland fires have gradually garnered attention, because CO<sub>2</sub> is the principal greenhouse gas. Globally, fires from the terrestrial biosphere are a major source of atmospheric carbon, occurring on a seasonal cycle and with substantial interannual variability. As early as the 1950s and 1960s, scientists began investigating the products emitted from burning wood, grass and crops to determine their effects on atmospheric environmental pollution. Initially, the environmental effects of combustion in household furnaces were investigated using a single-chamber furnace (Baes et al., 1976). In the 1970s, given the significant increase in CO<sub>2</sub> concentrations resulting from the extensive use of fossil fuels, several researchers began to investigate the increase in global CO<sub>2</sub> concentrations, the 'geochemical carbon cycle', 'the effects of increased CO<sub>2</sub> concentrations on climate change' and 'the effects of climate change on humans and their environment' (Possell et al., 2005). Grassland fires are a sudden and highly destructive natural disaster. Global warming and El Niño events have increased the frequency and intensity of grassland fires. Grassland fires generate large quantities of smoke, which is subsequently released into the atmosphere, thereby having a significantly negative impact on global warming, biogeochemical cycles, air quality and human health. Not only will grassland fires alter the structure, function, pattern and processes of the landscape, but they will also affect the carbon cycle and distribution of carbon in ecosystems (Conard and Solomon, 2008). Most parameters used in models of grass-

land fire carbon emissions are obtained from laboratory simulations, field observations, models or empirical estimations. Due to the diverse sources of these parameters, the accuracy of the estimates for carbon emissions is very uncertain. As technology continuously develops various remote sensing platforms provide data, and the corresponding algorithms are used extensively to retrieve the characteristic parameters to estimate carbon emissions from fires at a large scale (Tett et al., 1999; Crowley, 2000). Remote sensing technology, combined with models that estimate carbon emissions from fires, provide a new approach and means to estimate global carbon emissions from fires (Reister, 1984; De Groot, 2006; Groot et al., 2007; French et al., 2011; Shi et al., 2014). The highest emissions from fires have been caused by the burning of dry deciduous forests, followed by moist deciduous forests (Prasad et al., 2002). Remote sensing data have been used to analyze large-scale (Advanced Very High Resolution Radiometer, AVHRR data) (Kasischke et al., 1995; Chander et al., 2009), medium-scale (Moderate Resolution Imaging Spectroradiometer, MODIS data) and small-scale (Landsat Thematic Mapper, TM/Enhanced Thematic Mapper Plus, ETM+ data) grassland fires. The design of a wildfire monitoring system that incorporates wireless sensors and the results from field testing during prescribed test burns near San Francisco, California have been reported (Doolin et al., 2005). Clearly, wireless sensor networks (WSN) provide a viable solution for wildfire monitoring.

Grassland areas in China account for 6%–8% of the grassland areas in the world (Ni, 2002). The Inner Mongolia Grassland is the main temperate grassland in the north of China, accounting for 25% of the grassland area in China (Ni, 2002). It is of great significance to study the carbon emissions from fires of the Inner Mongolia Grassland in the context of better understanding the carbon cycle and carbon storage in the world. In the period 1981–2000, a total of 4266 forest and grassland fires occurred in the Inner Mongolia Autonomous Region, averaging 213.3 fires per year (Wen and Shen, 2008). Grassland fires are a unique and important ecological activity in ecosystems and an important disturbance factor that leads to dynamic changes in carbon stocks and emissions. On a global scale, many researchers have studied wildfires and their carbon emission estimates (Lasslop and Kloster, 2015) including the es-

timation of carbon emissions from wildfires in northern Eurasia, the relationship between grassland fires and climate (Liu et al., 2017) and the effects of land use on the occurrence of grassland fires (Li et al., 2017). Researchers have studied extensively the grassland fires of the Inner Mongolia Autonomous Region and have covered topics including the temporal and spatial dynamics of grassland fires (Zheng et al., 2013; Zhang et al., 2017), simulations of how grassland fires spread (Yang et al., 2008; Zhao et al., 2010), and the risks associated with grassland fires (Liu et al., 2010; Liu et al., 2015). Some researchers have studied the carbon cycle in the Inner Mongolia Grassland Ecosystem including the spatial characteristics of the soil organic carbon and nitrogen stocks in grasslands (Kanury, 1972; Ling, 1998), the effects of underground carbon sequestration in typical grassland and the changes to the grassland biomass. Additionally, researchers have used MODIS data and products to reconstruct the areas that were burned and to analyze the temporal and spatial patterns of fire disturbances in eastern Mongolia.

The Intergovernmental Panel on Climate Change (IPCC) designed a method to estimate a country's CO<sub>2</sub> emissions based on the consumption and carbon content of carbonaceous fossil fuels. However, for these estimates the method failed to include carbon emissions from grassland fires. Few studies have been conducted to estimate carbon emissions from grassland fires. It is important to accurately calculate carbon emissions from fires occurring in the grasslands of Inner Mongolia, to strengthen research on the global warming effects of grassland fire disturbances on carbon cycles and emissions from grassland ecosystems, to accurately evaluate the role of fire disturbance on the global carbon cycle and balance, to improve our understanding of the effects of fire disturbances on carbon cycles, to improve the sustainable management of grassland ecosystems and to employ more effective methods for managing the carbon balance in ecosystems.

At present, there are few studies on the estimation of carbon emissions which focus just on grassland fires (Cheng and Mikami, 2001; Ni, 2002); and a method for estimating direct carbon emissions (Soja et al., 2004) is mainly used to obtain the carbon emission parameters of the grasslands. The Global Wildland Fire Emission Model (GWEM) and other models have been used by

some researchers to estimate the carbon emissions from wildfire burning of all vegetation types in the world (including the Mongolian Plateau) based on monthly or annual scale simulations (Hoelzemann et al., 2004; Schultz et al., 2008). Otherwise, researchers obtain such data via field sampling, biomass measurement, carbon content measurement and greenhouse gas release, *etc.* (Soja et al., 2004; Hu et al., 2009). However, there is no general model for estimating carbon emissions from grassland fires. Satellite remote sensing data provide an effective means for estimation of the regional and global biomass (Hall et al., 1995; Moreau et al., 2003). At present, the estimations of carbon emissions are mainly based on experiments to determine the carbon emission of combustibles, the carbon content of combustibles, the combustion rate and other parameters (Liu and Tian, 2011; Hu et al., 2012), such that the total carbon emissions are estimated after grassland fire combustion by combining the above ground biomass data estimated by remote sensing (Liu and Tian, 2011; Wang et al., 2014). Therefore, the indoor combustion experiments are combined to measure the rate of carbon emissions and the combustion rate. The grassland aboveground biomass and the grassland fire carbon emission are estimated by field experiments and remote sensing data in Inner Mongolia.

This study has established an empirical relationship model based on ground sampling data and experimental combustion data, combined with remote sensing data, which can be used as a reference for estimating carbon emissions from grassland fires in other areas. The primary objectives of this study are to quantitatively investigate the parameters of carbon emissions associated with typical grasslands in Inner Mongolia through laboratory experiments and remote sensing methods, in order to estimate accurately the carbon emissions from grassland fires in Inner Mongolia, and to produce accurate maps of the spatial distribution of carbon emissions from grassland fires in Inner Mongolia for each year and determine the temporal and spatial patterns of change in carbon emissions from the fires in Inner Mongolia. Such estimates can provide reference data for quantitative evaluation of the role of carbon emissions originating from fires in the carbon balance of grassland ecosystems and reduce the uncertainties in estimations of the carbon balance in regional and global change research.

## 2 Materials and Methods

### 2.1 Study area

The Inner Mongolia Autonomous Region ( $37^{\circ}24'N$ – $53^{\circ}23'N$ ,  $97^{\circ}12'E$ – $126^{\circ}04'E$ ), situated in northern China and bordering Heilongjiang, Jilin and Liaoning to the east, Hebei, Shanxi and Ningxia to the south, Gansu to the west and Mongolia and Russia to the north, stretches approximately 2400 km from east to west and approximately 1700 km from south to north and extends from the northeast to the southwest in a narrow, long strip (Fig. 1).

This region has a temperate continental monsoon climate with an annual average temperature of  $0$ – $8^{\circ}C$  and an annual precipitation of 50–450 mm. Overall, the climate in this region is characterized by large temperature variations, numerous hours of sunshine and low and uneven precipitation. In addition, this region has a dry spring season with little precipitation, sharply rising temperatures and predominantly windy weather. Summers are tepid and short with concentrated precipitation and rapid plant growth. Thereafter, the temperature decreases sharply; a large diurnal temperature variation, early frosts and cold and dry snow-covered winters are

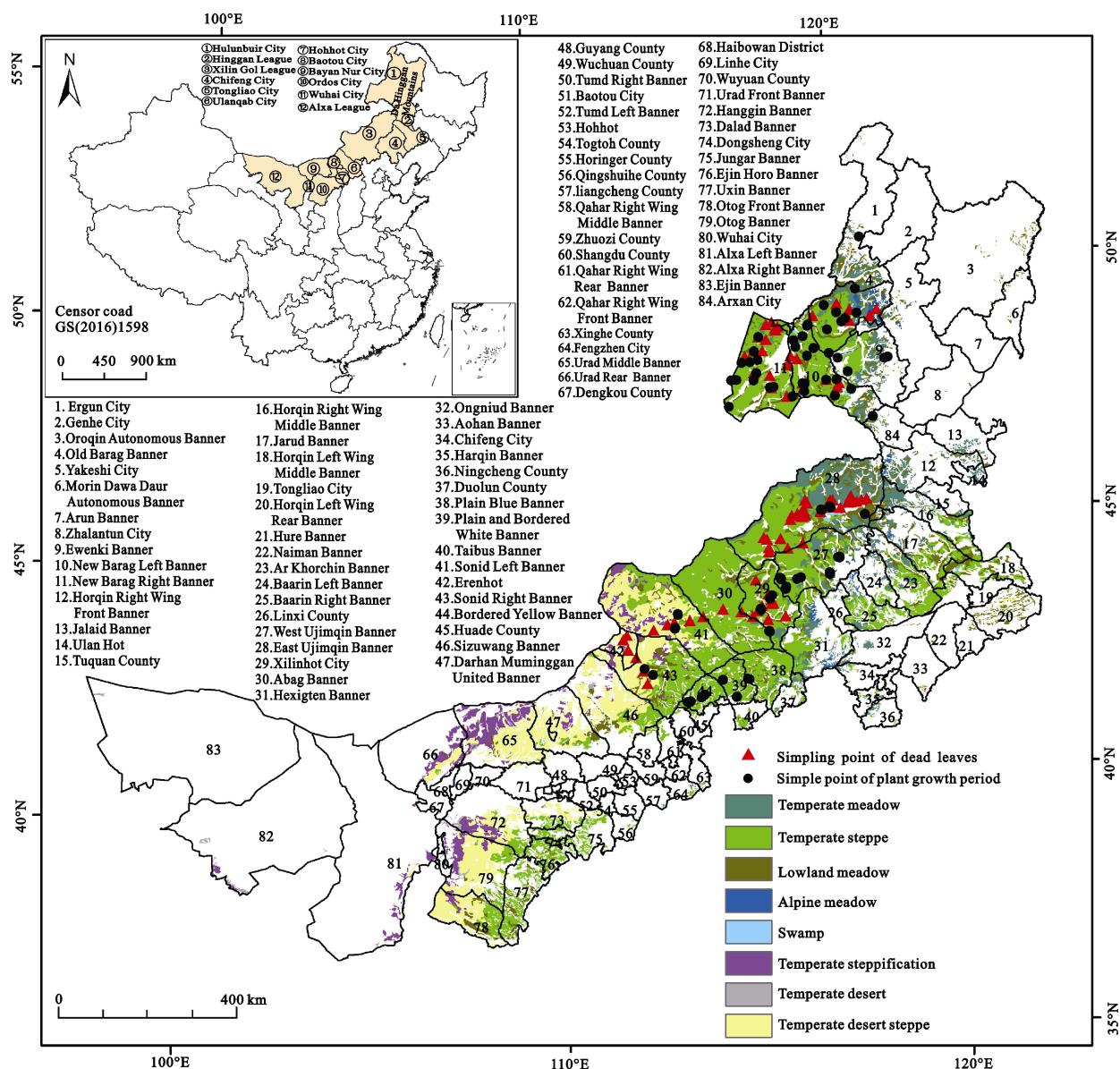


Fig. 1 Location of Inner Mongolia in China and distribution of grassland types and sampling points

common. Cold spells occur often. As a result of natural factors (e.g., landforms, climate and soil), the three vegetation types, namely, temperate meadow grassland, typical temperate grassland and temperate desert grassland, are distributed in a notable zonal pattern which extends from the northeast to the southwest of Inner Mongolia. The entire Inner Mongolia region has a total grassland area of 788 000 km<sup>2</sup> (Zhao and Xu, 2000). The main vegetation types in the study area include *Leymus chinensis*, *Stipa capillata*, *Cleistogenes squarrosa* and *Carex doniana*. Featuring a vulnerable ecological environment, Inner Mongolia is one of the world's regions most sensitive to climate change.

## 2.2 Research materials

### 2.2.1 Material acquisition

Fuel combustion is one of the largest sources of greenhouse gas emissions and plays a vital role in carbon and nitrogen chemical cycles. Based on grassland data and growing conditions, specific fire distribution areas were selected for study. Sample plots were established in typical grassland vegetation areas at relatively uniform spatial distribution; the individual sampling points were selected along roads in areas less affected by humans and were representative of the relatively large grassland vegetation areas of East Ujimqin Banner, Xilinhot, Abag Banner, Sonid Left Banner, Sonid Right Banner, Erenhot, Old Barag Banner, New Barag Left Banner and New Barag Right Banner (Fig. 1). To more effectively measure the surface fuel loads (the dry weights of aboveground biomass), 79 sampling points were selected randomly from grasslands that differed in coverage based on the distribution of vegetation burned in grassland fires, and their locations were determined using a handheld Garmin eTrex Vista global positioning system receiver. Field surveys and sampling were conducted during the growing season (June to August) in 2013, 2014 and 2016. Five repeat quadrats of 1 m × 1 m were established along a diagonal of each standard sample plot. The type, coverage and average height of vegetation in each quadrat were determined. Subsequently, the vegetation was cut flush with the ground and then weighed and sampled. Within the same study area during the non-growing season (November to April of the following year), the dry weights of aboveground biomass were collected from 1 m × 1 m quadrats in 2013, 2014 and 2016 and subsequently weighed and

sampled. The vegetation samples were dried at a constant temperature (70°C) and then weighed. The 70% of the ground survey data is used to participate in the calculation of regression equation, and the remaining 30% are used to verify the accuracy of regression equation.

### 2.2.2 Remote sensing data

The Normalized Difference Vegetation index (NDVI) and the Enhanced Vegetation Index (EVI) data (<https://search.earthdata.nasa.gov/>, temporal resolution: 16 d; spatial resolution: 500 m × 500 m) were extracted from the Moderate Resolution Imaging Spectroradiometer (MODIS) MOD13A1 product. The algorithm for this product selects the best available pixel value from all the acquisitions from the 16-day period. The criteria used are low clouds, low view angle, and the highest NDVI/EVI value. Provided along with the vegetation layers and two quality assurance (QA) layers are reflectance bands 1 (red), 2 (near-infrared), 3 (blue), and 7 (mid-infrared), as well as four observation layers. Land Surface Temperature (LST) data (land processes distributed active archive center, temporal resolution: 8 d; spatial resolution: 1 km × 1 km) were extracted from the MOD11A2 product. The MOD11A2 data were provided along with the daytime and nighttime surface temperature bands and associated quality control assessments, observation times, view zenith angles, and clear-sky coverages along with bands 31 and 32 for the emissivities from land cover types. Data on the areas burned were extracted using a 500-m monthly MODIS Burned Area Product MCD45A (a Version 5 MODIS land data product) released by the Land Processes Distributed Active Archive Center of the United States Geological Survey. The data from the MCD45A for the period 2000–2016 were compared with the results obtained using the disturbance index algorithm in terms of spatial distribution and range. The MCD45A Burned Area Product was produced by calculating the burned area, which is the difference between the change in the spectral reflectance time series for the target pixel and the normal condition based on a threshold value, using a bidirectional reflectance distribution function model and the continuous multiday reflectance and angle data (Boschetti et al., 2010).

Being an important link in the application of MODIS data, data quality control is an effective guarantee for the reliability and accuracy of research results. Through quality control, we can filter out the cloud, mixed cloud,

filled or missing data. The quality control layer in the MOD13A1 and MOD11A2 data used in this study is 16-bit unsigned integer data, with decimalization as its default storage mode. Before use, this data needs to be converted to binary, and then the files that can be used as quality control files are extracted according to the MODIS vegetation index user's guide. For the MOD13A1 data, bits 2–5 in the binary data represent the availability of the VI based on the product manual. In the manual, 0000 represents the highest quality which we consider as the mask layer to extract the NDVI data. For the MOD11A2 data, bits 2–3 digits in the binary representation of the data quality mark, where 00 represents good data quality data, are considered as the mask layer to extract the LST data. The MCD45A data contain a quality evaluation layer that conducts storage using 8-bit unsigned integers. A value of 0 in the 0 position represents a water pixel, and a value of 1 represents land. A value of 1 in the 1 position represents valid data, and 0 represents unverified data. We used the land and the valid data as mask layers, to extract and obtain the

data for the area burned.

## 2.3 Methods

### 2.3.1 Research framework

In this study, a model for estimating carbon emissions from grassland fires was established via burning experiments of surface samples and quantitative remote sensing data. Fig. 2 presents the technical flowchart of this study.

### 2.3.2 Acquisition method for emission rate of carbon

Surface fuel loads of grassland can be converted to the carbon stock equivalent. The carbon stock of grassland is generally estimated by multiplication directly or indirectly by measuring the standing vegetation surface fuel loads by their carbon content. In this study, the ignition time, rate of heat release, rate of mass loss and emitted gases (including CO and CO<sub>2</sub>) were measured using a cone calorimeter. In the stipulated ambient conditions (relative humidity: 30%; temperature: 20°C), the entire vegetation samples were dried at 70°C to constant weight. Samples of each grassland type were ground

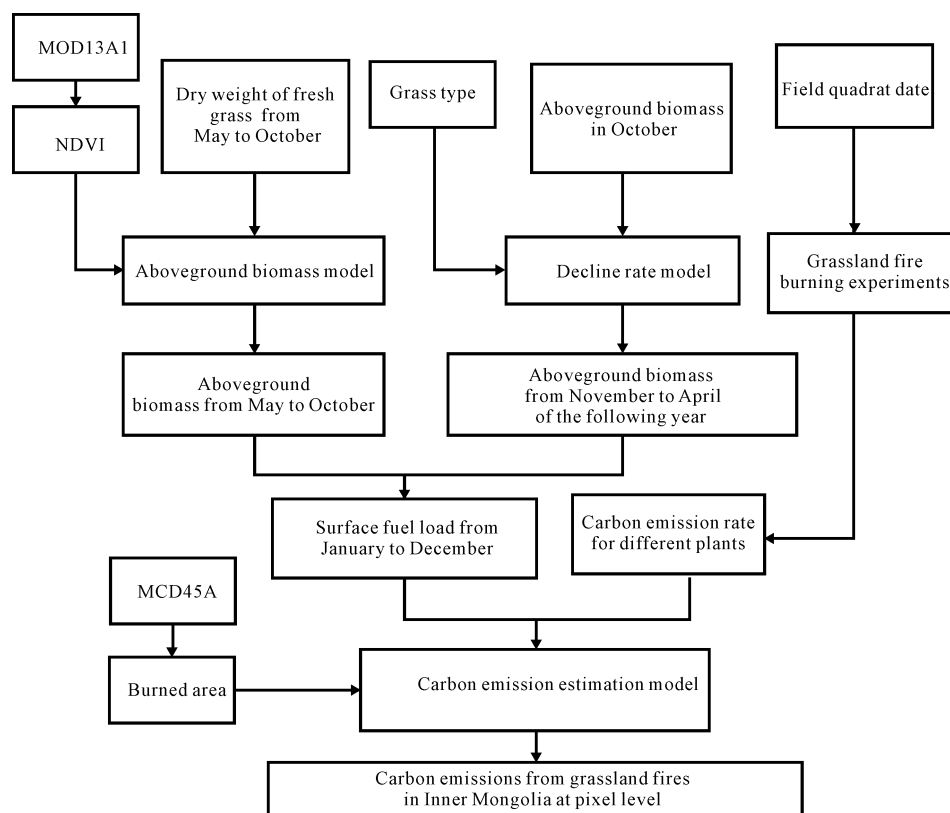


Fig. 2 Research framework of carbon emissions from grassland fire in Inner Mongolia, China

using a micro-plant grinding machine. The resultant samples were sieved through a 100-mesh sieve and prepared as specimens, which were then stored at room temperature for subsequent analysis. The cone calorimeter required the specimen to have a square shape with sides of length 100 mm. Thus, the specimen size was set to 100 mm × 100 mm. The weight of each specimen was 2 g. All test specimens were exposed in a homogeneous environment. A standard pilot ignition device was used as the guiding device. For each specimen, all sides, except for the top, were covered with 0.03–0.05 mm thick aluminum foil, which was permitted to exceed its top surface by at least 3 mm. In addition, heat transfer from the back of each sample to the external environment was prevented using asbestos to reduce the effects of the external environment. To allow the experimental temperature to be close to the actual temperature, according to the ASTM E1354-90 standard, the thermal radiation flux, the radiation distance and the corresponding temperature were set to 25 kW/m<sup>2</sup>, 25 cm and approximately 488.9°C, respectively, and the gas exhaust flow was adjusted to (0.024 ± 0.002) m<sup>3</sup>/s. The experiment was started after a balance was reached. Three repeats were conducted. The values for each index were averaged. The CO and CO<sub>2</sub> emission rates were converted to emissions per unit mass. In the burning experiments, to better reflect spatial carbon emissions, sampling points with the same type of vegetation were merged.

### 2.3.3 Calculation of surface fuel load

In this study, the surface fuel load during the growing season was calculated (Eq. (1)) by the dry weights of aboveground biomass, and during the non-growing season was calculated based on the surface fuel load in October and the decline coefficient.

$$F_{ij} = \begin{cases} A_{ij}, j = 5, 6, 7, 8, 9, 10 \\ B_{ij}, j = 11, 12, 1, 2, 3, 4 \end{cases} \quad (1)$$

where  $F_{ij}$  is the total surface fuel load of pixel  $i$  in month  $j$ ;  $A_{ij}$  is the total surface fuel load of pixel  $i$  from May to October;  $B_i$  is the total surface fuel load of pixel  $i$  from November to April of the next year;  $i$  is the pixel,  $j$  is the month.

The dry weight of aboveground biomass per unit area was determined for various types of grassland from the 1 m × 1 m quadrats from June to August of 2013, 2014

and 2016. In addition, the MODIS NDVI data corresponding to the sampling points were also used. Based on the remote sensing NDVI data and dry weight of aboveground biomass, a unitary nonlinear regression model was established (Eq. (2)), as follows:

$$A_{ij} = 410 \times NDVI_{ij}^{1.45} \quad (2)$$

where  $A_{ij}$  is total surface fuel load of pixel  $i$  in month  $j$ ;  $NDVI_{ij}$  is the NDVI value of pixel  $i$  in month  $j$ ;  $i$  is the pixel,  $j$  is the month.

The dry weights of the aboveground biomass obtained from the 1 m × 1 m quadrat from November of 2013, 2014 and 2016 to April of the following year were used as the surface fuel loads for these periods. Based on the dry weights of the aboveground biomass data and month, a unitary linear regression model was established for different grassland types (Eq. (3)), as follows:

$$y = ax + b \quad (3)$$

where the  $y$  represents the dry weight of aboveground biomass data in ground; the  $x$  equal to 1, 2, 3, 4, 5, 6 representative November to May of the next year,  $a$  is the monthly decline coefficient of different grassland types (Table 1),  $b$  is the intercept of different grassland types.

Based on the surface fuel load for October calculated using equation in Equation (2), the surface fuel load in November to April of the next year were calculated (Eq. (4)), when the surface fuel load is less than 0, we set it to 0. as follows:

$$B_{ij} = \begin{cases} ax + A_{i10}, B_{ij} \geq 0 \\ 0, B_{ij} < 0 \end{cases} \quad (4)$$

where the  $B_{ij}$  is the surface fuel load of pixel  $i$  in month  $j$ ; the  $x$  equal to 1, 2, 3, 4, 5, 6 representative November to May of the next year;  $a$  is the monthly decline coefficient of different grassland types (Table 1);  $A_{i10}$  is the dry weight of aboveground biomass in October;  $i$  is the pixel,  $j$  is the month.

### 2.3.4 Calculation of carbon emissions

Seiler and Crutzen (1980) proposed a method for calculating the surface fuel load lost in a grassland fire. Several researchers (Kasischke et al., 1995; Running, 2006) further developed this method and considered in detail the contributions to carbon emissions from aboveground

**Table 1** The decline coefficient of different grassland types

Grassland types	<i>a</i>
<i>Stipa capillata</i>	-17.32
A combination of <i>Stipa grandis</i> and <i>Leymus chinensis</i>	-3.89
A combination of <i>Stipa klemenzii</i> and <i>Cleistogenes squarrosa</i>	-4.77
A combination of <i>Filifolium sibiricum</i> and <i>Stipa grandis</i>	-4.07
<i>Leymus chinensis</i>	-1.37
A combination of <i>Leymus chinensis</i> and <i>Stipa grandis</i>	-2.15
A combination of <i>Leymus chinensis</i> and <i>Poa annua</i>	-4.71
A combination of <i>Leymus chinensis</i> and <i>Caragana sinica</i>	-2.86
<i>Stipa grandis</i>	-15.01
A combination of <i>Leymus chinensis</i> and <i>Stipa klemenzii</i>	-31.06
A combination of <i>Stipa grandis</i> and <i>Caragana sinica</i>	-11.53
A combination of <i>Stipa grandis</i> and <i>Cleistogenes squarrosa</i>	-9.03
<i>Caragana sinica</i>	-19.26
A combination of <i>Caragana sinica</i> and <i>Stipa klemenzii</i>	-12.11
<i>Stipa krylovii</i>	-5.19
A combination of <i>Stipa krylovii</i> and <i>Caragana sinica</i>	-1.14
<i>Poa annua</i>	-3.46
A combination of <i>Stipa klemenzii</i> and <i>Caragana sinica</i>	-0.63
A combination of <i>Stipa klemenzii</i> and <i>Cleistogenes squarrosa</i>	-3.01
A combination of <i>Stipa klemenzii</i> and <i>Dendranthema</i>	-0.29
A combination of <i>Stipa klemenzii</i> and <i>Artemisia scoparia</i>	-2.66
Others	-7.12

Note: *a* is the monthly decline coefficient of different grassland types

surface fuels (trees, bushes and herbaceous vegetation), surface litter, humus and coarse woody debris (Choi et al., 2006). These previous studies included in the models the combustion efficiency of forest fires for emission of carbon. Given that grasslands are mostly consumed during forest fires, the combustion efficiency is taken as 100%, which has no effect on our research model. In this study, an expression (Equation (5)) for carbon emissions from grassland fires was obtained based on the data acquired from the burning experiments conducted using the cone calorimeter as follows:

$$C_i = A_i \times F_i \times \sum_{j=1}^5 (W_{ijk} \times R_{ijk}) \quad (5)$$

where  $C_i$  is the total carbon emissions from the burning of surface fuels of pixel  $i$  (g);  $A_i$  is the area burned of pixel  $i$ ;  $F_i$  is the surface fuel load of pixel  $i$ ;  $W_{ijk}$  is the percentage of plants  $j$  in grass  $k$ ; and  $R_{ijk}$  is the carbon emission rate (Table 2) of plants  $j$  in grass (Table 1)  $k$ ;  $j$  is the main plants of *Leymus chinensis*, *Stipa capillata*, *Cleistogenes squarrosa* and *Carex doniana* and mean value of others grass.

**Table 2** Carbon emissions from combustion of different plants (carbon emissions per 1 g plant)

Grass	Carbon emissions rate	Grass	Carbon emissions rate
<i>Taraxacum mongolicum</i>	0.82	<i>Picris hieracioides</i>	0.10
<i>Orostachys fimbriata</i>	0.60	<i>Adenophora gmelinii</i>	0.10
<i>Leymus chinensis</i>	0.45	<i>Ephedra sinica</i>	0.10
<i>Vicia sepium</i>	0.43	<i>Inula britannica</i>	0.09
<i>Silene conoidea</i>	0.41	<i>Artemisia scoparia</i>	0.09
<i>Ptilotricum canescens</i>	0.38	<i>Agropyron cristatum</i>	0.08
<i>Stipa capillata</i>	0.37	<i>Saussurea japonica</i>	0.08
<i>Lactuca sibirica</i>	0.34	<i>Allium bidentatum</i>	0.08
<i>Saposhnikovia divaricata</i>	0.32	<i>Artemisia capillaris</i>	0.08
<i>Allium ramosum</i>	0.27	<i>Artemisia dalai-lamae</i>	0.08
<i>Chenopodium album</i>	0.27	<i>Adeinophora stricta</i>	0.08
<i>Artemisia sieversiana</i>	0.24	<i>Oxytropis myriophylla</i>	0.07
<i>Echinops sphaerocephalus</i>	0.24	<i>Thalictrum petaloideum</i>	0.07
<i>Thymus mongolicus</i>	0.23	<i>Ephedra sinica</i>	0.06
<i>Scorzonera ruprechtiana</i>	0.23	<i>Artemisia frigida</i>	0.06
<i>Serratula centauroides</i>	0.21	<i>Iris lactea</i>	0.06
<i>Haplophyllum dauricum</i>	0.21	<i>Allium polyrhizum</i>	0.05
<i>Melissitus ruthenicus</i>	0.2	<i>Gentiana squarrosa</i>	0.05
<i>Carex doniana</i>	0.187	<i>Polygala tenuifolia</i>	0.05

Continued Table 2

Grass	Carbon emissions rate	Grass	Carbon emissions rate
<i>Cleistogenes squarrosa</i>	0.187	<i>Stellera chamaejasme</i>	0.05
<i>Androsace umbellata</i>	0.18	<i>Haplophyllum dauricum</i>	0.04
<i>Astragalus mongholicus</i>	0.18	<i>Polygonum</i>	0.04
<i>Asparagus cochinchinensis</i>	0.18	<i>Iris tectorum</i>	0.04
<i>Convolvulus ammannii</i>	0.17	<i>Allium tuberosum</i>	0.04
<i>Oxytropis mollis</i>	0.17	<i>Chamaerhodos erecta</i>	0.03
<i>Brassica oleracea</i>	0.17	<i>Lespedeza bicolor</i>	0.03
<i>Salsola collina</i>	0.15	<i>Caragana sinica</i>	0.03
<i>Mosla chinensis</i>	0.15	<i>Chenopodium album</i>	0.03
<i>Poa annua</i>	0.13	<i>Potentilla acaulis</i>	0.03
<i>Neopallasia petinata</i>	0.13	<i>Allium chrysanthum</i>	0.02
<i>Convolvulus ammannii</i>	0.13	<i>Bupleurum chinense</i>	0.02
<i>Gypsophila davurica</i>	0.12	<i>Filifolium sibiricum</i>	0.02
<i>Peucedanum harry-smithii</i>	0.11	<i>Plantago asiatica</i>	0.01
<i>Heteropappus altaicus</i>	0.1	<i>Gentiana squarrosa</i>	0.01

### 3 Results

#### 3.1 Model validation

To verify the over-fitting of the modeling process, it is necessary to verify the accuracy of surface fuel load estimation model. The surface fuel load retrieved from remote sensing and the dry weight of aboveground biomass measured in the field were compared as shown in Fig. 3 with  $R^2 = 0.767$  ( $P < 0.0001$ ), which shows that the aboveground biomass retrieved from remote sensing data was acceptable.

#### 3.2 Spatial and temporal distribution patterns of surface fuel loads

The annual average surface fuel load of the grasslands in Inner Mongolia during 2000–2016 was calculated to be approximately  $1.1978 \times 10^{12}$  kg (Fig. 4). Fig. 4 shows that the surface fuel load as the grassland type decreased from temperate meadow grassland to temperate grassland to temperate desert grassland, from east to west. Over the entire study area, relatively high surface fuel loads appeared in the foothill area west of the Da Hinggan Mountains and gradually decreased toward the Xilin Gol Plateau and the Ulanqab Plateau. The surface fuel loads per unit area in Xilin Gol League, Ulanqab City and Hohhot City located north of  $43^\circ\text{N}$  exceeded those south of  $43^\circ\text{N}$ . However, due to the undulating relief of the mountainous region, the surface fuel loads were distributed in an irregular manner. Except for the foothill area of the Da Hinggan Mountains, the surface fuel load per unit area

decreased from northeast to southwest. As shown in Fig. 5, the surface fuel load increased during the period 2000–2016 and reached a high value in 2013 and a low value in 2007. Evidently, the surface fuel load varied significantly between the different years of the studied period.

#### 3.3 Spatial and temporal distribution patterns for burned grassland areas

The total grassland area burned in the Inner Mongolia region from 2000 to 2016 was  $5298.75 \text{ km}^2$ , with an annual average area of  $311.69 \text{ km}^2$  (Fig. 6). Cumulatively, the area burned in 2000, 2001, 2003, 2005, 2012, 2013 and 2014 accounted for 81.99% of the total area burned over the 17-year period.

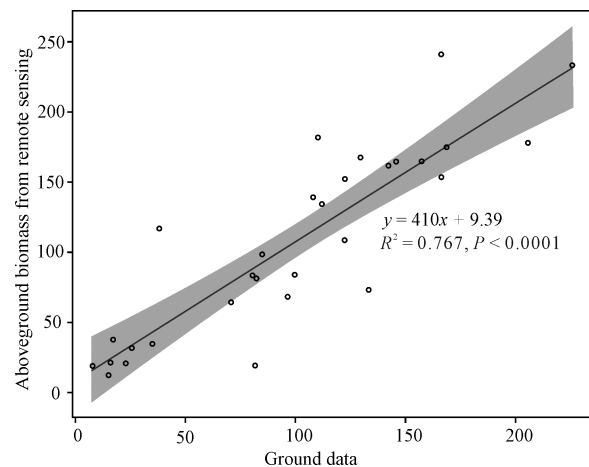


**Fig. 3** Comparison of aboveground biomass of grassland retrieved from the remote sensing data and measured through the field data in Inner Mongolia in 2013, 2014 and 2016

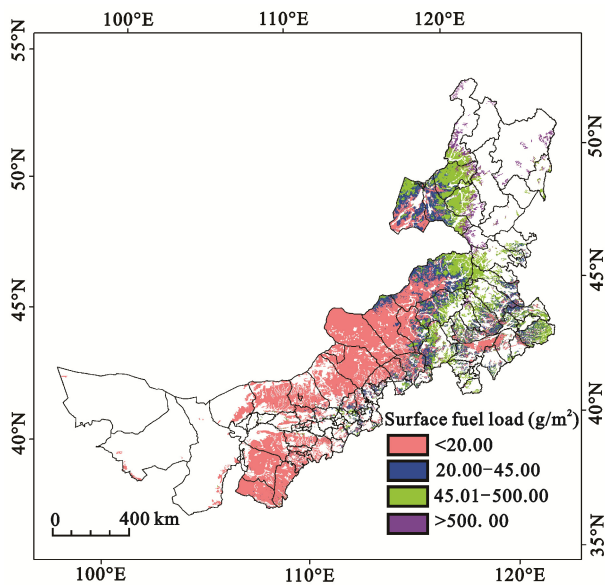


**Fig. 4** Annual average of surface fuel loads for the grasslands of Inner Mongolia during 2000–2016

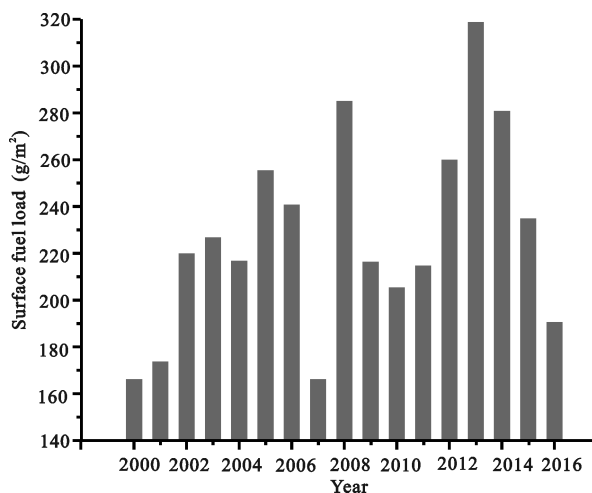


**Fig. 5** The variability in the surface fuel loads of the grasslands of Inner Mongolia during the period 2000–2016

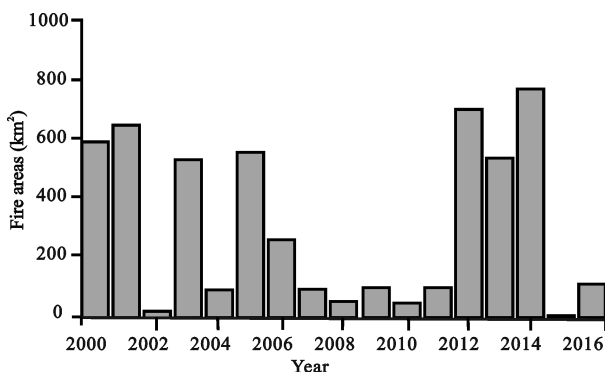


**Fig. 6** Area of grassland burned in Inner Mongolia during 2000–2016

The grassland areas burned in Inner Mongolia were primarily concentrated along the border between China, Russia and Mongolia. It was distributed in several administrative districts, namely, Hulunbuir City, Hinggan League, Xilin Gol League and Ulanqab City. Based on the distribution of surface fuel loads, large areas which were burned occurred where surface fuel loads were concentrated. Fire-prone areas were located on the leeward slopes of the Da Hinggan Mountains, which primarily has centrally distributed grasslands and low precipitation. The fires were stoked by the northwestern monsoon on its windward slopes. As a result of fires spreading, fires occurred at a high rate along the border between China and Mongolia. However, given China's timely monitoring of grassland fires, those fires that occurred along the border were extinguished quickly. As depicted in Fig. 7, the fire points were relatively scattered at the junction of Qahar Right Wing Front Banner, Zhuozi County and Fengzhen City, districts under the jurisdiction of Ulanqab, at the junction of Qahar Right Wing Front Banner and Qahar Right Wing Rear Banner and the junction of Taibus Banner and Plain Blue Banner south of Xilin Gol, Oroqen Autonomous Banner west of the Da Hinggan Mountains and Morin Dawa Daur Autonomous Banner. These fire points occurred mainly in March and April of 2014. Based on the surface fuel load in 2014 ( $61.2 \times 10^4$  kg) and the population distribution, these fires were caused by the burning of straw on farmland in spring. Relatively few grasslands were distributed west of the Da Hinggan Mountains. However, the proportion of the burned area west of the Da Hinggan Mountains was high.

### 3.4 Temporal and spatial distribution patterns for carbon emissions

The carbon emissions from grassland fires in Inner Mongolia and their rate of change calculated using the model of carbon emissions from fires are presented in Eq. (4). The total carbon emissions in the Inner Mongolia region during 2000–2016 amounted to  $2.24 \times 10^7$  kg, with an annual average of  $1.32 \times 10^6$  kg (Fig. 8). Overall, grassland carbon emissions during the period 2000–2016 decreased slightly, principally as a result of China's monitoring activities and timely interventions (Fig. 8). These results show that the cumulative carbon emissions in 2000, 2003 and 2005 accounted for 43.77% of the total carbon emissions. In 2000, the grassland

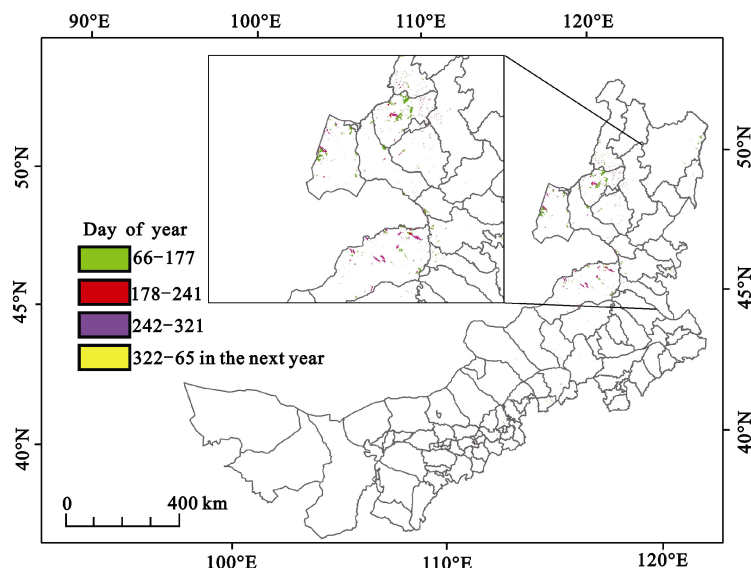


Fig. 7 The timing of grassland fires during the period 2000–2016

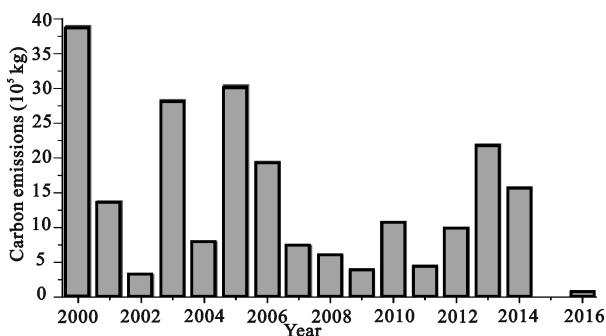


Fig. 8 Carbon emissions from the grasslands of Inner Mongolia during the period 2000–2016

area burned was 593.75 km<sup>2</sup> resulting the carbon emission was  $3.91 \times 10^6$  kg (Fig. 6). In 2005, the area burned was 562.25 km<sup>2</sup>, and the carbon emission was  $3.05 \times 10^6$  kg.

As illustrated in Table 4, there was a strong correlation between carbon emissions and the areas subjected to fires. The data show that the larger the area of the fire, the greater the carbon emissions.

The spatial distribution of carbon emission per unit area in red and purple colors reflect the highest values of carbon emissions (Fig. 9). High carbon emissions were main distributed in Old Barag Banner and New Barag left Banner and on the right side of the Oroqin Autonomous Banner (Fig. 9). Carbon emissions in East Ujimqin Banner, New Barag Right Banner and Arxan City

were distributed mainly along the border. In other areas, carbon emissions were distributed in an irregular manner. By enlarging the areas with centrally distributed carbon emissions, high carbon emissions per unit pixel were found along the border between China Mongolia and Russia, particularly in East Ujimqin Banner. China has relatively low grassland surface fuel loads and monitors grassland fires in a timely manner. As a consequence, there have been relatively low carbon emissions from grassland fires during the study period. It can be seen that high-carbon emission areas are located in the eastern and central part of the map and low-carbon emission areas are located toward the west (Fig. 10). Old Barag Banner and East Ujimqin Banner have the highest total carbon emission, more than  $3.0 \times 10^6$  kg. The blank area represents no fire, so the carbon emission in this area is 0.

Table 4 Correlation matrix between carbon emissions, fuel load and fire area

Name	Carbon emissions (kg)	Surface fuel load (kg)	Fire area (ha)
Carbon emissions (kg)	1.000		
Surface fuel load (kg)	0.170	1.000	
Fire area (ha)	0.684**	0.301**	1.000

Note: \*\* significant at the 0.01 level (both sides)

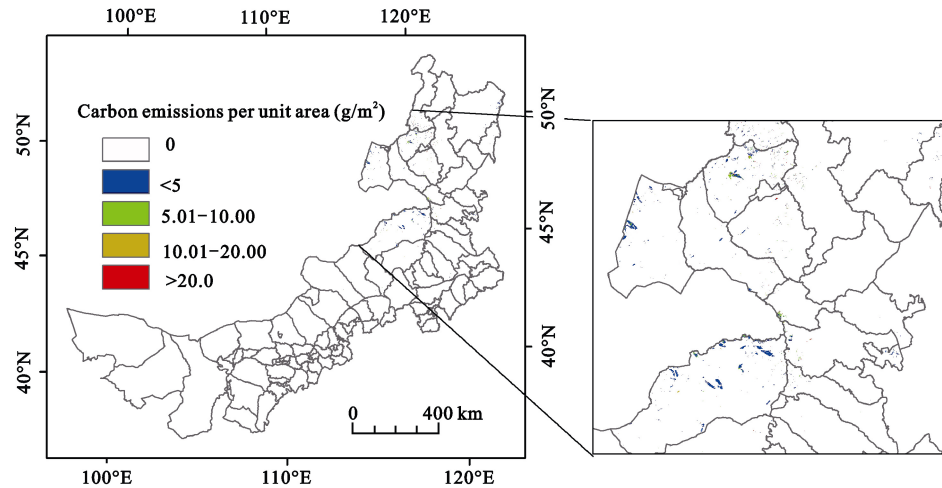


**Fig. 9** The carbon emissions per unit area in the grasslands of Inner Mongolia during the period 2000–2016

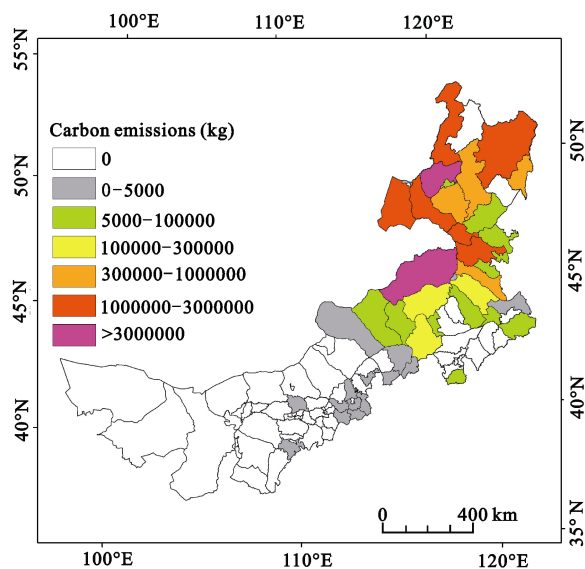


**Fig. 10** The total carbon emissions in the grasslands of Inner Mongolia during the period 2000–2016

## 4 Discussion

### 4.1 Estimation of carbon emission

There are some uncertainties in the accuracy of the estimations of carbon emissions (Lasslop and Kloster, 2015), due to the diversity in the sources of parameters used for calculation. The amount of grassland fuel provides the basis for the calculation. The estimation of the combustible quantity requires an appropriate model for the combustible quantity to be selected. For large-scale research, especially global research, it is difficult to find an appropriate model that describes all combustible

types in the study area. Most of the estimation parameters for carbon emissions are obtained by methods such as laboratory simulation, field observation, model simulation or estimation based on experience (Lehsten et al., 2009; Lasslop and Kloster, 2015). A combustible quantity model is not robust enough to apply to China, thus for the present study the carbon emission rate for various grassland types in Inner Mongolia Grassland were obtained by the indoor carbon emission experiments. The results of such an approach can provide empirical coefficients for combustibles in other areas with the same type of grassland. The combustibles after drying to constant weight were used for combustion experiments, but when actual grassland fires occur, the grassland combustibles may not actually have been dry. In order to make the data more reliable, the combustion characteristics of combustibles with different moisture contents can be tested, and the climatic conditions when the grassland fire occurred can be taken account to improve the accuracy of estimation. As a result of ground sampling, the weight of grassland per unit area can be used to estimate the combustible load and the proportion of grassland types in the sample plot. Given the complexity of vegetation types in the grassland, it is difficult to obtain and assess all vegetation types when selecting the sampling points. In the study, only a proportion of main grassland types were calculated. For minor grassland types, these are treated as other types, which introduce uncertainty to the results. Increasing the quantity of sampling points to cover more vegetation types can make up for this deficiency. The MODIS data, which

featured a resolution of 500 m in this study, contained many types of grassland, which would have a certain effect on the results when estimating the total carbon emissions. Use of multi-source remote sensing data fusion and data assimilation technology with high spatial-temporal resolution and high spectral resolution can improve the estimation accuracy for remote sensing of carbon emissions from grassland fires.

## 4.2 Factors influencing carbon emissions from grassland fires

The carbon emissions from grassland fires are usually governed by the combustion area, the combustible load, the combustion efficiency and the meteorological conditions at the time of the fire (Lehsten et al., 2009; Lasslop and Kloster, 2015). The large areas of grassland fires in Inner Mongolia are mainly concentrated in the grassland areas in the middle eastern parts of Inner Mongolia (Fig. 7), and are primarily due to the prevalence of the north-westerly winds in the spring and autumn. The forest grassland fires in Mongolia and Russia can be readily spread to the study area, which causes grassland fires in the border areas to be typically of high frequency, long duration and covering a large area. There is a strong correlation between the amount of carbon emissions from grassland fires and the observed fires for the study area. In the years when there was a large area of fires, the amount of carbon emissions was large, such as in 2000 and 2005. The carbon emissions in these two years were significantly higher than in other years, and the area of fires in these two years was higher than that in other years (Fig. 6). However, the carbon emissions were not proportional to the areas of the fires; and the spatial locations of the fires were also a particularly important factor. For example, the year with the most carbon emissions over the past 17 yr was 2000, but the fire area in that year was lower than that in 2014. Therefore, from consideration of the fire area and the spatial location of the combustible load in these two years, it can be inferred that the fires were mainly governed by the spatial distribution of the combustible load. It can be noted that the amount of combustible grassland and its temporal and spatial distribution play an important role in the occurrence of the fire. A small amount of combustible grassland is not sufficient to support the spread and dispersion of the fire and the carbon emissions will increase with an increase in the per-unit-area combustible

load. The continuous expansion of prohibited grazing areas and grazing-free areas and the effective restoration of grassland vegetation are the most important factors that control the annual change of the combustible load. At the same time, implementation of the Green for Grain Project in Xilin Gol League, Ulanqab City, Baotou City and other places in Inner Mongolia has also greatly changed the aboveground biomass (Peters and Verhoeven, 1994). Influenced by the Pacific monsoon, the grassland climate and vegetation in Inner Mongolia have changed significantly from northeast to southwest. In typical grassland, semi desert grassland and desert grassland, with a decrease in precipitation, the aboveground biomass ratio of grassland communities shows a downward trend (Fan et al., 2009). The amount and spatial distribution of the combustible quantity in grassland are affected by regional hydrothermal conditions and other meteorological factors. Different grassland types and grassland coverage will affect the combustion efficiency of grassland, which, in turn, affect the carbon emissions. Meteorological factors also have a great impact on the combustion efficiency of grassland combustibles. Humid weather conditions lead to inadequate combustion of combustibles, so that the aboveground biomass of grassland cannot be fully transferred into carbon emissions. At the same time, meteorological factors are important factors in the simulation of grassland fire occurrences and spread. In the case of the presence of grassland combustibles and fire sources, whether the grassland can catch fire and whether it can spread after catching fire mainly depends on the meteorological conditions at that time, such as high temperature, less precipitation, low relative humidity, strong wind, drought, *etc.* Therefore, in the process of grassland fire carbon emission simulation, inputting the meteorological conditions at that time will increase the accuracy of estimation.

## 4.3 Uncertainty

The temporal and spatial distribution of organisms in the study area exhibits heterogeneity and is also affected by the interactions of various factors. In previous studies, these parameters were often assumed to be homogeneous, i.e., these parameters were considered unchanged in a certain region to simplify the analysis. In this study, the sampling points were classified based on the quadrat data measured on the ground and grassland map at a

scale of 1 : 1 000 000. However, due to their limited number, the sampling points did not cover all types of vegetation. There are two primary methods for determining surface fuel loads, namely, ground surveys and remote sensing imagery. Surface fuel load data are affected by the interactions of several factors. In addition, a uniform standard for obtaining measured surface fuel load data is still lacking. As a result, the research methods used by different researchers vary greatly. Currently, typical surface fuel load studies mainly use models and regression equations (Choi *et al.*, 2006; Yin *et al.*, 2009). A suitable surface fuel load model is required to estimate surface fuel loads. However, for large-scale studies, particularly for global studies, it is difficult to identify a suitable model to describe the combustion characteristics of all the surface fuels within a study area. Further research is required to investigate the correlations between the surface fuel load, the intermediate characteristic parameters and the remote sensing retrieval method to more accurately estimate surface fuel loads.

The applicability of characteristic indices which relate to the areas burned varies when applied to different regions, vegetation types and seasons. It is necessary to study comprehensively the characteristics of the various types of indices and investigate, on a collaborative basis, the extraction methods for the area burned. Grassland surface fuels are the material consumed in grassland fires and surface fuel loads are the basis for measuring carbon emissions from fires. There are two main methods for determining the surface fuel loads, namely, ground surveys and remote sensing estimation. Surface fuel load data are affected by the interactions of various factors. In addition, a uniform standard for obtaining measured surface fuel load data is still lacking. As a result, a large difference exists among research methods. Surface fuel loads vary seasonally due to changes in vegetation productivity and decomposition rates and the time and frequency of fires. In this study, an estimation model for carbon emissions from grassland fires in Inner Mongolia was established using remote sensing retrieval combined with ground experiments; this model can be used to estimate carbon emissions from grassland fires in large areas and provides a reference for estimating carbon emissions from global-scale grassland fires. It is necessary to study the uncertainty factors to improve the accuracy of carbon emission estimation. In future research, to increase the accuracy of estimates of surface

fuel loads, it will be necessary to use high-temporal and spatial resolution, high-spectral resolution multisource remote sensing data fusion and data assimilation techniques to provide new approaches and methods for accurately extracting the key parameters (e.g., surface fuel load) for estimates of carbon emissions from grassland fires derived from remote sensing imagery. In addition, it will be necessary to study surface fuel load-related environmental factors (e.g., meteorological factors) and to establish more accurate relationship models. Furthermore, the surface fuel load models for China are currently inadequate and it will thus be necessary to establish reliable, practical fuel models that can meet the remote sensing application requirements for China's surface fuel load distribution system. In future studies, to improve the accuracy of estimates of the fuel load, it will be necessary to adopt multisource remote sensing data fusion and data assimilation technology with high spatial and temporal resolution and high spectral resolution to detect carbon emissions of grassland fires remotely. Accurate estimation of key parameters provides new ideas and methods, and further study of environmental factors will aid in the establishment of a more accurate model.

## 5 Conclusions

Taking Inner Mongolia grassland in China as the research area, we obtain the carbon emissions per unit area of designated grassland type through carbon emission combustion experiments of different grassland types. Then the surface fuel load was calculated based on the above ground biomass and remote sensing NDVI data. Based on a model for estimating carbon emissions from fires, the temporal and spatial changes in surface fuel load and carbon emissions from grassland fires in Inner Mongolia were analyzed. The main conclusions are as follows:

- (1) The annual average surface fuel load of the grasslands in Inner Mongolia during 2000–2016 was calculated to be approximately  $1.1978 \times 10^{12}$  kg, the surface fuel load reached a high value in 2013 and a low value in 2007. The high surface fuel loads appeared in the foothill area west of the Da Hinggan Mountains and gradually decreased toward the Xilin Gol Plateau and the Ulanqab Plateau.

- (2) The total grassland area burned in the Inner

Mongolia region from 2000 to 2016 was 5298.75 km<sup>2</sup>, with an annual average area of 311.69 km<sup>2</sup>. The grassland areas burned in Inner Mongolia were primarily concentrated along the border between China, Russia and Mongolia. The large areas which were burned occurred where surface fuel loads were concentrated.

(3) Total carbon emissions from fires for the grasslands of Inner Mongolia between 2000 and 2016 amounted to  $2.24 \times 10^7$  kg with an annual average of  $1.32 \times 10^6$  kg. Interannual carbon emissions changed insignificantly and slightly decreased. The carbon emissions in year 2000, 2003 and 2005 were higher than those of more normal years. Carbon emissions decreased gradually from east to west and were particularly pronounced in the border area west of the Da Hinggan Mountains and the border area of East Ujimqin Banner.

## References

- Baes C F Jr, Goeller H E, Olson J S et al., 1976. *The Global Carbon Dioxide Problem*. Oak Ridge National Laboratory, ORNL-5194, Oak Ridge, Tennessee.
- Boschetti L, Roy D P, Justice C O et al., 2010. Global assessment of the temporal reporting accuracy and precision of the MODIS burned area product. *International Journal of Wildland Fire*, 19(6): 705–709. doi: 10.1071/WF09138
- Chander G, Markham B L, Helder D L, 2009. Summary of current radiometric calibration coefficients for Landsat MSS, TM, ETM+, and EO-1 ALI sensors. *Remote Sensing of Environment*, 113(5): 893–903. doi: 10.1016/j.rse.2009.01.007
- Choi S D, Chang Y S, Park B K, 2006. Increase in carbon emissions from forest fires after intensive reforestation and forest management programs. *Science of the Total Environment*, 372(1): 225–235. doi: 10.1016/j.scitotenv.2006.09.024
- Conard S G, Solomon A M, 2008. Chapter 5 Effects of wildland fire on regional and global carbon stocks in a changing environment. *Developments in Environmental Science*, 8: 109–138. doi: 10.1016/S1474-8177(08)00005-3
- Crowley T J, 2000. Causes of climate change over the past 1000 years. *Science*, 289(5477): 270–277. doi: 10.1126/science.289.5477.270
- de Groot W J, 2006. Modeling Canadian wildland fire carbon emissions with the Boreal Fire Effects (BORFIRE) model. *Forest Ecology and Management*, 234: S224. doi: 10.1016/j.foreco.2006.08.251
- de Groot W J, Landry R, Kurz W A et al., 2007. Estimating direct carbon emissions from Canadian wildland fires. *International Journal of Wildland Fire*, 16(5): 593–606. doi: 10.1071/WF06150
- Doolin D M, Sitar N, 2005. Wireless sensors for wildfire monitoring. In *Smart Structures and Materials 2005: Sensors and Smart Structures Technologies for Civil, Mechanical, and Aerospace Systems. International Society for Optics and Photonics*, 5765: 477–484. doi: 10.1117/12.605655
- Fan J W, Wang K, Harris W et al., 2009. Allocation of vegetation biomass across a climate-related gradient in the grasslands of Inner Mongolia. *Journal of Arid Environments*, 73(4–5): 521–528. doi: 10.1016/j.jaridenv.2008.12.004
- Feng Q, Cheng G D, Mikami M, 2001. The carbon cycle of sandy lands in China and its global significance. *Climatic Change*, 48(4): 535–549. doi: 10.1023/A:1005664307625
- Flannigan M D, van Wagner C E, 1991. Climate change and wildfire in Canada. *Canadian Journal of Forest Research*, 21(1): 66–72. doi: 10.1139/x91-010
- French N H F, de Groot W J, Jenkins L K et al., 2011. Model comparisons for estimating carbon emissions from North American wildland fire. *Journal of Geophysical Research: Biogeosciences*, 116(G4): G00K05. doi: 10.1029/2010JG001469
- Hall F G, Townshend J R, Engman E T, 1995. Status of remote sensing algorithms for estimation of land surface state parameters. *Remote Sensing of Environment*, 51(1): 138–156. doi: 10.1016/0034-4257(94)00071-T
- Hoelzemann J J, Schultz M G, Brasseur G P et al., 2004. Global Wildland Fire Emission Model (GWEM): evaluating the use of global area burnt satellite data. *Journal of Geophysical Research: Atmospheres*, 109(D14): D14S04. doi: 10.1029/2003JD003666
- Hu Haiqing, Wang Guangyu, Sun Long, 2009. Analyses of gas emission in ground covers combustion of main forest fuel types in Xiaoxing'an Mountain. *Scientia Silvae Sinicae*, 45(5): 109–114. (in Chinese)
- Hu Haiqing, Wei Shujing, Jin Sen et al., 2012. Measurement model of carbon emission from forest fire: a review. *Chinese Journal of Applied Ecology*, 23(5): 1423–1434. (in Chinese)
- Hu Haiqing, Wei Shujing, Sun Long et al., 2013. Interaction among climate change, fire disturbance and ecosystem carbon cycle. *Arid Land Geography*, 36(1): 57–75. (in Chinese)
- Kanury A M, 1972. Thermal decomposition kinetics of wood pyrolysis. *Combustion & Flame*, 18(1): 75–83. doi: 10.1016/S0010-2180(72)80228-1
- Kasischke E S, French N H F, Bourgeau-Chavez L L et al., 1995. Estimating release of carbon from 1990 and 1991 forest fires in Alaska. *Journal of Geophysical Research*, 100(D2): 2941–2951. doi: 10.1029/94JD02957
- Lasslop G, Kloster S, 2015. Impact of fuel variability on wildfire emission estimates. *Atmospheric Environment*, 121: 93–102. doi: 10.1016/j.atmosenv.2015.05.040
- Lehsten V, Tansey K, Balzter H et al., 2009. Estimating carbon emissions from African wildfires. *Biogeosciences*, 6(3): 349–360. doi: 10.5194/bg-6-349-2009
- Li Linghao, Liu Xianhua, Chen Zuozhong, 1998. Study on the carbon cycle of *Leymus chinensis* steppe in the Xilin River Basin. *Acta Botanica Sinica*, 40(10): 955–961. (in Chinese)
- Li Y P, Zhao J J, Guo X Y et al., 2017. The influence of land use on the grassland fire occurrence in the Northeastern Inner

- Mongolia autonomous region, China. *Sensors*, 17(3): 437. doi: 10.3390/s17030437
- Liu Bin, Tian Xiaorui, 2011. Carbon emission from Huzhong forest fire in Daxing'anling. *Forest Resources Management*, (3): 47–51. (in Chinese)
- Liu M F, Zhao J J, Guo X Y et al., 2017. Study on climate and grassland fire in HulunBuir, Inner Mongolia autonomous region, China. *Sensors*, 17(3): 616. doi: 10.3390/s17030616
- Liu X P, Zhang J Q, Tong Z J, 2010. The dynamic danger assessment for grassland fire disaster in Xilingol, Inner Mongolia. *Computational Intelligence: Foundations and Applications*, 1110–1116. doi: 10.1142/9789814324700\_0171
- Liu X P, Zhang J Q, Tong Z J, 2015. Modeling the early warning of grassland fire risk based on fuzzy logic in Xilingol, Inner Mongolia. *Natural Hazards*, 75(3): 2331–2342. doi: 10.1007/s11069-014-1428-5
- Moreau S, Bosseno R, Gu X F et al., 2003. Assessing the biomass dynamics of Andean *bofedal* and *titora* high-protein wetland grasses from NOAA/AVHRR. *Remote Sensing of Environment*, 85(4): 516–529. doi: 10.1016/S0034-4257(03)00053-1
- Ni J, 2002. Carbon storage in grasslands of China. *Journal of Arid Environments*, 50(2): 205–218. doi: 10.1006/jare.2201.0902
- Peters A, Verhoeven K J F, 1994. Impact of artificial lighting on the seaward orientation of hatchling loggerhead turtles. *Journal of Herpetology*, 28(1): 112–114. doi: 10.2307/1564691
- Possell M, Nicholas Hewitt C, Beerling D J, 2005. The effects of glacial atmospheric CO<sub>2</sub> concentrations and climate on isoprene emissions by vascular plants. *Global Change Biology*, 11: 60–69. doi: 10.1111/j.1365-2486.2004.00889.x
- Prasad V K, Gupta P K, Sharma C et al., 2002. CO and CO<sub>2</sub> emissions from biomass burning of tropical dry deciduous and mixed deciduous forests in shifting cultivation areas of India. *Pollution Research*, 21(2): 143–155. doi: 10.1016/S0140-6701(03)82155-0
- Reister D B, 1984. The use of a simple model in conjunction with a detailed carbon dioxide emissions model. *Energy*, 9(8): 637–643. doi: 10.1016/0360-5442(84)90092-6
- Rodhe H, 1990. A comparison of the contribution of various gases to the greenhouse effect. *Science*, 248(4960): 1217–1219. doi: 10.1126/science.248.4960.1217
- Running S W, 2006. CLIMATE CHANGE: is global warming causing more, larger wildfires?. *Science*, 313(5789): 927–928. doi: 10.1126/science.1130370
- Schultz M G, Heil A, Hoelzemann J J et al., 2008. Global wildland fire emissions from 1960 to 2000. *Global Biogeochemical Cycles*, 22(2): GB2002. doi: 10.1029/2007GB003031
- Shi Y S, Sasai T, Yamaguchi Y, 2014. Spatio-temporal evaluation of carbon emissions from biomass burning in Southeast Asia during the period 2001–2010. *Ecological Modelling*, 272: 98–115. doi: 10.1016/j.ecolmodel.2013.09.021
- Soja A J, Cofer W R, Shugart H H et al., 2004. Estimating fire emissions and disparities in boreal Siberia (1998–2002). *Journal of Geophysical Research*, 109(D14): D14S06. doi: 10.1029/2004JD004570
- Tett S F B, Stott P A, Allen M R et al., 1999. Causes of twentieth-century temperature change near the Earth's surface. *Nature*, 399(6736): 569–572. doi: 10.1038/21164
- Tian Xiaorui, Shu Lifu, Wang Mingyu, 2003. Direct carbon emissions from Chinese forest fires, 1991–2000. *Fire Safety Science*, 12(1): 6–10. (in Chinese)
- Van der Werf G R, Randerson J T, Giglio L et al., 2010. Global fire emissions and the contribution of deforestation, savanna, forest, agricultural, and peat fires (1997–2009). *Atmospheric Chemistry and Physics*, 10: 11707–11735. doi: 10.5194/acp-10-11707-2010
- Villars P, Cenzual K, 2011. *Space Groups* (140) *I4/mcm*–(136) *P42/mnm*. Berlin: Springer.
- Wang Xinyun, Guo Yige, He Jie, 2014. Estimation of above-ground biomass of grassland based on multi-source remote sensing data. *Transactions of the Chinese Society of Agricultural Engineering*, 30(11): 159–166. (in Chinese)
- Wen Kegang, Shen Jianguo, 2008. *Chinese Meteorological Disasters Ceremony (Inner Mongolia Volume)*. Beijing: China Meteorological Press. (in Chinese)
- Yang H Y, Zhao C, Liu Y W, 2008. GIS-based Inner Mongolia grassland fire spread simulation system. In: *2008 International Conference on Computer Science and Software Engineering*. Hubei, China: IEEE, 923–925. doi: 10.1109/CSSE.2008.764
- Yin Li, Tian Xiaorui, Kang Lei et al., 2009. Research development of carbon emissions from forest fires. *World Forestry Research*, 22(3): 46–51. (in Chinese)
- Zhang Z X, Feng Z Q, Zhang H Y et al., 2017. Spatial distribution of grassland fires at the regional scale based on the MODIS active fire products. *International Journal of Wildland Fire*, 26(3): 209–218. doi: 10.1071/WF16026
- Zhao C, Meng K Q L, Yang H Y, 2010. The design and realization of Inner Mongolia grassland fire spread simulation system based on GIS and CA. In: *2009 1st International Conference on Information Science and Engineering*. Nanjing, China: IEEE, 2205–2208. doi: 10.1109/ICISE.2009.1197
- Zhao Mengli, Xu Zhixin, 2000. Rational use of grassland resources and sustainable development of animal husbandry in Inner Mongolia. *Resources Science*, 22(1): 73–76. (in Chinese)
- Zheng Wei, Shao Jiali, Wang Meng et al., 2013. Dynamic monitoring and analysis of grassland fire based on multi-source satellite remote sensing data. *Journal of Natural Disasters*, 22(3): 54–61. (in Chinese)